Journal of Power Sources 240 (2013) 736–744

Contents lists available at SciVerse ScienceDirect

Journal of Power Sources

journal homepage: www.elsevier.com/locate/jpowsour

Spray-assisted silar deposition of cadmium sulphide quantum dots on metal oxide films for excitonic solar cells

I. Concina [a,*], N. Memarian [a,b], G.S. Selopal [a], M.M. Natile [c], G. Sberveglieri [a], A. Vomiero [a]

[a] SENSOR Laboratory, CNR-IDASC & Brescia University, Via Branze 45, 25133 Brescia, Italy
[b] Physics Department, Semnan University, Semnan, Iran
[c] CNR-ISTM and Department of Chemical Sciences, University of Padova, via Marzolo 1, 35131 Padova, Italy

HIGHLIGHTS

- Application of spray deposition to SILAR quantum dots generation is presented.
- Enhanced optical density of CdS quantum dots on TiO_2 is achieved.
- Smaller nanocrystal sizes were systematically obtained.
- Improved functional features of quantum dot sensitized solar cells were recorded.

GRAPHICAL ABSTRACT

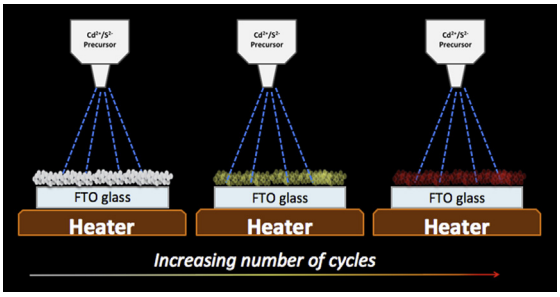

ARTICLE INFO

Article history:
Received 8 March 2013
Received in revised form
22 April 2013
Accepted 9 May 2013
Available online 20 May 2013

Keywords:
Spray deposition
SILAR
Semiconductor-sensitized solar cells
Quantum dot growth kinetics

ABSTRACT

The proof of principle of the successful application of spray deposition to the SILAR (successive ionic layer absorption and reaction) technique, one of the most effective strategies to sensitized TiO_2 scaffold with QDs, is demonstrated. Systematically improved optical features of the materials (higher optical density together with reduced nanocrystal sizes) as well as of the functional performances of QD solar cells (photoconversion efficiency, fill factor, short circuit current, open circuit voltage) sensitized via SD-SILAR, with respect to traditional SILAR sensitization based on impregnation, are demonstrated.

1. Introduction

Inorganic semiconductor nanocrystals (NCs), also known as quantum dots (QDs) have attracted a remarkable interest over the last two decades as appealing materials to be exploited in a variety of domains [1–3]. This attention is especially motivated by their optical and electronic properties, easily tunable through the modulation of their dimensions. The first paper dealing with their preparation appeared in 1993 [4] and since then many efforts have been carried out devoted to both increase the basic knowledge on these systems and the ways to exploit them.

In particular, in the field of third generation photovoltaics (PV), semiconductor QDs appear as the ultimate frontier as light harvesters [3], since they have band gap easily tunable with sizes, they can energetically sensitize metal oxides, they can expand the solar spectrum region in which light is collected [5] and they could in principle overcome the Queisser–Shockley limit, thanks to the claimed multiexciton generation effect, the presence of intraband transitions and other processes, which are not present in single

* Corresponding author.
E-mail address: isabella.concina@ing.unibs.it (I. Concina).

0378-7753/$ – see front matter © 2013 Elsevier B.V. All rights reserved.
http://dx.doi.org/10.1016/j.jpowsour.2013.05.012

junction cells [6]. Unfortunately, up to now the performances provided by quantum dot sensitized solar cells (QDSCs) are still lower as compared with those shown by classical dye sensitized solar cells [7]; QDSCs are indeed photoelectrochemical systems very different from their homologues DSCs, although taking advantage from a very similar architecture, and many things are to be learnt from the very beginning [8,9]. However, this has not reduced the tremendous interest for QDSCs and many efforts are currently carried out to understand these systems and building up devices with improved performances. Very recently, a remarkable 5.4% photoconversion efficiency has been obtained with Mn-doped CdS/CdSe QDs [10]. From the technological viewpoint, the same research group set-up a one-step coating approach to design relatively high efficiency semiconductor-sensitized solar cells, based on QD-sensitized TiO_2 paint [11].

Over the last three years, the technique known as SILAR (successive ionic layer adsorption and reaction) has emerged as an effective strategy to directly generate and grow semiconductor QDs on a host surface. This approach is particularly promising in the field of QDSCs for which increased photoconversion efficiencies (PCEs) have been obtained [12–14].

SILAR technique presents several appealing advantages as compared with the classical synthetic approaches, based on the well-known hot injection method. It is indeed a very simple and fast strategy to generate semiconductor nanocrystals, envisaging a certain number of immersion/washing/drying cycles into ionic solutions of selected precursors. According to the number of cycles and the chosen precursors, it is also easily possible growing QDs of various sizes and building up networks of different materials, thus opening the path towards the so-called rainbow QDSCs. SILAR approach provides for polydisperse QDs and allows an intimate contact between them and the metal oxide surface used as host (typically, a thin film of nanoparticulate TiO_2).

On the other hand, some limits related to the SILAR technique in the field of PV have also been highlighted: a faster recombination with respect to colloidal QDs and a decrease in the rate of photogenerated electron injection with the number of SILAR cycles [15]. Despite the mentioned limits, SILAR remains an interesting way to easily exploit QDs for PV.

A real scenario technological exploitation of these materials asks for development of synthetic routes able to provide low cost, high production yield, high reproducibility, precise control of composition and size, low by-products amount. This latter point is of particular relevance, taking into account that the chosen materials are often composed of heavy metals (such as cadmium) and, in view of the possibility to scale up the production, waste should be as reduced as possible.

In this work we propose an innovative synthetic route to fabricate semiconductor quantum dots of CdS on polycrystalline TiO_2 scaffold via SILAR technique mediated by spray deposition (SD-SILAR). The approach has been recently attempted in literature for generation of CdS QDs, exploiting secondary sulphide sources (such as thiourea), needing thermal decomposition to provide for S^{2-} ions [16]. This mandatory treatment requires temperatures as high as 400–450 °C and in some cases a post-growth annealing devoted to either eliminate big CdS aggregates or improve QD attachment on TiO_2 scaffold [17], resulting in undesired CdO formation.

In the present study, growth dynamics at low temperatures (RT to 60 °C) and QD features obtained by applying the two SILAR approaches are systematically studied and compared, demonstrating improved functional features of the QDs obtained via SD-SILAR with respect to traditional SILAR technique based on impregnation and reaction in a hot application such as a QDSC. Moreover, we will show that the SD-SILAR approach uses quite reduced amount of precursor materials, without any waste.

CdS QDs have been chosen as system models, since they are easily generated and grown on metal oxide surface with simple procedures, without any need for operating in inert atmosphere, and they are among the most exploited semiconductor sensitizers in QDSCs.

2. Experimental

2.1. Preparation of photoanode

The photoanodes were prepared by tape casting commercial TiO_2 pastes (from Dyesol) on FTO glass (sheet resistance $\sim 10\ \Omega\ \square^{-1}$), followed by 30 min annealing at 450 °C in air. Substrates with various thicknesses were applied, ranging from 2 μm up to 11.5 μm. In the case of thin substrates (up to 5 μm) transparent TiO_2 layer was applied (Dyesol 18 NR-T, composed of anatase nanoparticles 20 nm in diameter). The 11.5-μm thick layers have a bi-layered structure in which a 4-μm thick scattering layer (Dyesol WER2-O, composed of anatase particles 150 nm to 250 nm in diameter) is added to the 7.5 μm thick transparent one.

2.2. Deposition and optical characterization of QDs

A 0.05 M ethanolic solution of $Cd(NO_3) \times 4H_2O$ (Sigma Aldrich) and a 0.05 M solution of $Na_2S \times 9H_2O$ (>99.99%, Sigma Aldrich) in H_2O/MeOH (50/50) were used as sources of Cd^{2+} and S^{2-}, respectively. Bidistilled water (Carlo Erba), ethanol (>99.5%, Sigma Aldrich) and methanol (>99.9%, Sigma Aldrich) were used as solvent. All chemicals were used as received without any further purification. Traditional bath-SILAR was carried out by immersing the TiO_2 photoanode into the suitable precursor solution for 1 min, followed by washing the substrate and drying it with a slight nitrogen flux.

SD-SILAR was carried out by using a two-guns apparatus, working with nitrogen (6 psi) as carrier gas (nozzles-to-sample distance: 10 cm). Cd^{2+} and S^{2+} precursor solution were loaded in the respective gun reservoir and sprayed for a given time, according to the chosen volume to be deposited. When needed, the substrate was placed on a hot plate and heated at the desired temperature. Cadmium and sulphide precursors were then alternatively sprayed. After each precursor spraying, sample was washed and dried with the same procedure as adopted for traditional bath-SILAR. All photoanodes were capped with ZnS (1 SILAR cycle), using 0.1 M aqueous solutions of $Zn(CH_3COO)_2 \times 2H_2O$ (99.999% Sigma Aldrich) and $Na_2S \times 9H_2O$.

UV–Vis spectra of the sensitized photoanodes were recorded on a TG80 PG Instrument (1 nm resolution). QD sizes are calculated from UV–Vis absorption spectra on the basis of Eq. (1) [18]:

$$D = (-6.6521 \times 10^{-8})\lambda^3 + (1.9557 \times 10^{-4})\lambda^2 - (9.2352 \times 10^{-2})\lambda + (13.29) \quad (1)$$

2.3. XPS measurements

XPS measurements were run on a Perkin-Elmer PHI 5600ci spectrometer. The spectrometer was calibrated by assuming the binding energy (BE) of the Au $4f_{7/2}$ line to be 84.0 eV with respect to the Fermi level. Both extended spectra (survey – 187.85 eV pass energy, 0.5 eV/step, 0.025 s/step) and detailed spectra (for Cd 3*d*, S 2*p*, O 1*s*, Ti 2*p* and C 1*s* – 11.75 eV pass energy, 0.1 eV/step, 0.1s/step) were collected with a standard Al-Kα source (1486.6 eV) working at 250 W. The reported binding energies (BEs, standard deviation = ±0.1 eV) were corrected for the charging effects by considering the adventitious C1*s* line at 285.0 eV. The atomic

percentages, after a Shirley type background subtraction, were evaluated by using the PHI sensitivity factors [19].

2.4. Functional characterization

Cell fabrication was carried out using a sulphide/polysulfide mixture (S^{2-} 1M, S 1M, NaOH 0.1 M in bidistilled water) as electrolyte. The active area of the cells was 25 mm^2. Au-coated FTO (5 nm thick sputtered Au film) was used as the counter electrode with plastic spacer 25 μm thick. The functional properties of the cells were investigated under simulated sunlight irradiation using an ABET 2000 solar simulator at AM 1.5G (100 mW/cm^2), calibrated at one sun using a reference Si solar cell.

3. Results and discussion

CdS QDs are deposited on TiO_2 thin film by means of both classical immersion SILAR (hereafter bath-SILAR) and SD-SILAR. Every sample has been characterized by ultraviolet–visible (UV–Vis) spectrophotometry after each deposition cycle. It is well known that this technique is a powerful tool to investigate semiconductor QDs since their main spectral features (position of the first excitonic peak and related absorbance value) are directly correlated with nanocrystal size and amount, respectively [18]. While colloidal QDs show sharp excitonic peak, correlated with nanocrystals presenting focused size distribution, SILAR-deposited QDs have broad absorption bands, indicating a rather broad dispersion in size. This dispersion is attributed to the fact that SILAR-prepared QD are generated and grown as naked on a surface that acts as a host, determining their features through its own. However, increase in absorbance value as well as shift in excitonic band position still correlate with increasing nanocrystal amount and sizes [20].

The first impressive effect of SD-SILAR CdS QDs generation is shown in Fig. 1(a), in which a direct comparison between the optical features obtained for the same generation-and-growth number of cycles is reported for the two adopted approaches. For both the processes UV–Vis absorption spectra clearly indicate formation of QDs, according to the presence of a spread shoulder in the range 380 to 440 nm, whose intensity increases and position shifts towards larger wavelengths by increasing the number of SILAR cycles, due to augmented QD amount and size, respectively. SD-SILAR provides for CdS QDs with much higher optical density (OD) value. This trend is systematic for each cycle and can be fitted in both cases with a linear relation suggesting that both systems evolve according to the same mechanism, irrespectively of the deposition approach. Moreover, the increase in OD is faster for the SD-SILAR.

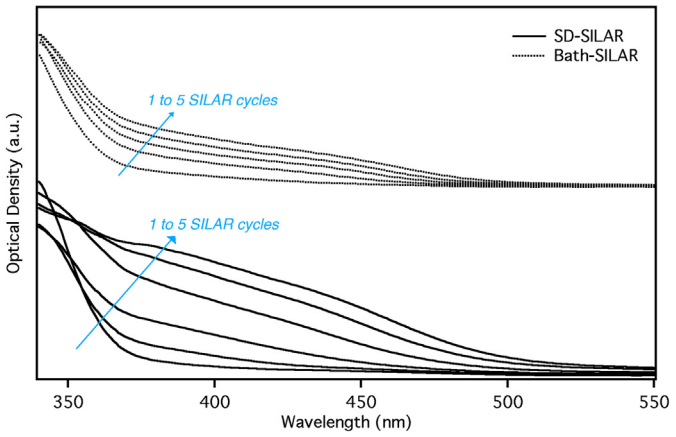

Fig. 1. Comparison between absorption features obtained for 1–5 generation cycles for SD-SILAR (solid line) and classical bath-SILAR (dotted line). *y* Axis has been rescaled for clarity purposes.

The influence of working conditions on both optical density and sizes of QDs produced via SD-SILAR has been systematically investigated, focusing on the volume of precursor solutions sprayed (0.1, 0.5 and 1.0 ml for each cycle) and on the temperature of the substrate (RT, 40, 50 and 60 °C).

The effect of the volume of precursor solution is shown in Fig. 2. As expected, a reduced amount of precursor solution (0.1 ml) results in reduced OD together with the smallest nanocrystal size. On the contrary, the use of 1 ml precursor provides for the highest sizes, but the OD keeps rather low, most probably due to an incomplete uptake of the precursor from the substrate surface. The substrate is instead able to incorporate the whole volume when 0.5 ml are sprayed, which were found to be the best amount, both providing for a complete uptake and resulting in an optimal OD as well as in high molar extinction coefficient and acceptable nanocrystal sizes. It is in particular worth noting that the values of extinction coefficients (calculated according to Ref. [18]), associated to the probability of an effective excitation, obtained for 0.5 ml and 1 ml volumes are comparable, confirming that half a milliliter is the optimal quantity to be used for a fine tuning of the sensitizers properties.

These effects can be understood in terms of both available mass precursor able to interact for QD formation and conformal coverage of the available area of the mesoporous network. Obviously, higher sprayed volume reflects in larger available feed material for QD growth. However, the dynamics of SILAR process has to be considered accurately to understand the resulting behavior of QD formation. SILAR is based on sequential absorption of a single precursor monolayer over the available surface. In traditional bath-SILAR the solution can be considered as an almost infinite precursor reservoir, which leads to conformal coverage of the available sample surface during each step (in a kind of saturated process) and the process dynamics is mainly driven by diffusion. In this respect, by keeping fixed the precursor concentrations, the optical density of the resulting layer is primarily determined by the roughness factor of the sample (i.e. the total available surface per sample area) and the number of SILAR cycles, which determines the fractional coverage of oxide surface by active ions for QD nucleation. In SD-SILAR the dependence of QD nucleation and QD size on precursor volume calls for incomplete coverage of available surface by sprayed precursor at least for 0.1 ml volume, allowing fine tuning of QD formation process as clearly demonstrated. OD evolution vs. the number of SILAR cycles is well fitted by a linear regression (whose parameters are listed in Table 1). The slope (which we will call kinetic constant, despite the expression would be not completely rigorous) remarkably increases as soon as the best volume amount is used, thus confirming the above discussion.

Moreover, the volume of the sprayed precursor influences also the rate of QD formation, as indicated by the fit parameters reported in Table 1.

QD formation is also dependent upon temperature, as reported in Fig. 3.

The first point worth noting is that the process still follows a linear trend in all cases for both SD- and bath-SILAR with the only exception of SD-SILAR carried out at 60 °C. This latter is no longer linear along with the number of cycles, being instead well fitted by an exponential trend.

Taking into account that plotting the OD is equivalent to consider the evolution of concentration of QDs, the growth of nanocrystals onto TiO_2 network appears to follow a zero order kinetics (first order for SD-SILAR at 60 °C).

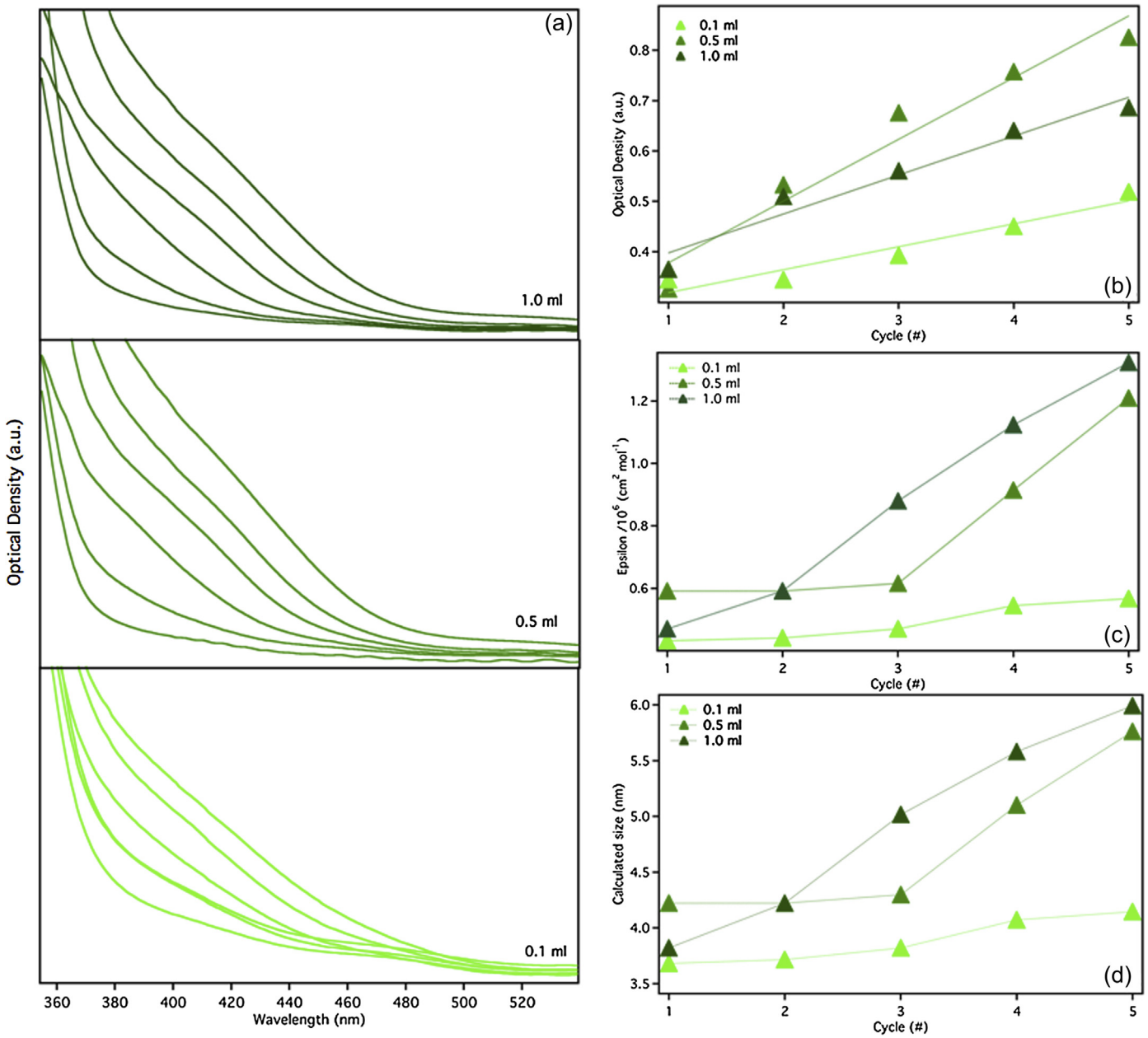

Fig. 2. Effect of the spray solution volume on (a) the absorption spectra of CdS QDs (bottom to top: 0.1 ml; 0.5 ml; 1.0 ml); (b) optical density; (c) molar extinction coefficient; (d) nanocrystal sizes. 0–5 SD-SILAR cycles are considered. Triangles: 0.1 ml; circles: 0.5 ml; squares: 1.0 ml.

It should be here remarked that the observed behavior is different from the growth kinetics identified for colloidal monodisperse nanocrystals grown by means of the hot injection approach and analogous synthetic methods. Some studies [21,22] have indeed demonstrated that, in such cases, the growth follows a self-catalytic path, in which the just-formed nanocrystals act as a catalyst towards the subsequent growth.

On the other hand, the same studies have highlighted that diameter growth is a two-step process, composed by a first, faster stage, followed by a slower one.

In the case of SILAR generation and growth, irrespectively from the process adopted (bath vs SD), growth dynamics follows a different mechanism. This finding could be ascribed to the fact that SILAR exploit a heterogeneous system (liquid for the chalcogenide precursor and solid for the substrate) that seems to orient the growth.

For each growth, the kinetic constant was then determined (see Table 1). A remarkable difference in the behavior of the systems clearly emerges from these calculations: increasing the temperature from 40 to 60 °C (very close to solvent boiling point) results in a slight decrease of the kinetic constant for the QDs deposited by bath-SILAR, whereas an opposite trend was evidenced for SD-SILAR-grown QDs. This feature can be understood in term of the thermal agitation caused by the temperature. Diffusion does not take advantage from these motions, which, on the contrary, reduce the interaction between the reservoir and the metal oxide network. This is better understood reminding again that the process in bath-SILAR is carried out in a heterogeneous system, in which only one component is free to move (the precursor solution), whereas its partner (the TiO_2 layer) is fixed on a substrate. It is worth mentioning that the opportunity of not increasing the sensitization temperature has also been recently remarked for DSCs by Gratzel's

Table 1
Fitting parameters for samples prepared using different parameters.

Parameter	Sample	Kinetic constant (cycles^{-1})	Correlation coefficient
Volume effect	0.1 ml	0.046	0.962
	0.5 ml	0.122	0.973
	1.0 ml	0.077	0.976
Temperature effect	Bath 25 °C	0.0468	0.964
	SD 25 °C	0.05146	0.983
	Bath 40 °C	0.0894	0.988
	SD 40 °C	0.0993	0.982
	Bath 50 °C	0.0742	0.987
	SD 50 °C	0.1427	0.999
	Bath 60 °C	0.0544	0.986
	SD 60 °C[a]	0.85936	–

[a] Exponential fit.

group [23], who ascribed the effect to an increased structural order of the composed system when lowering the temperature.

On the other hand, since in the case of SD the heating is furnished directly to the substrate (see Section 2), increasing the operating temperature turns out in speeding up the solvent evaporation thus favoring the process of precursors deposition. This is true in the range 25–50 °C, while a decrease in k was found when the substrate is heated up to 60 °C, which is extremely close to the boiling point of ethanol, and the system changes its kinetics.

Another important feature is the enhanced OD of SD-SILAR with respect to bath-SILAR, as clearly visible in Fig. 3. Above 50 °C, SD-SILAR exhibits an optical density more than double with respect to bath-SILAR. Such behavior is in line with previous results on QD size. Of course, reduced grain size of QDs allows close packed assembly with enhanced specific volume occupied by QDs, which reflects on OD (proportional to the volume of the absorbing medium); for this reason, reduced QD size (SD-SILAR) results in enhanced OD, with beneficial effects on light absorption and photoconversion efficiency.

The last effect of the temperature is related to the obtained nanocrystal sizes, which, as predictable, increased along with the temperature in both cases.

Key feature for exploitation of TiO_2-sensitized layers is homogeneous in-depth concentration of QDs, allowing uniform sensitization of the entire TiO_2 scaffold. EDS analysis (Fig. 4) on cross-sections of sensitized TiO_2 clearly indicates perfectly uniform in-depth profile for all monitored elements (i.e. Cd, S, Ti) in CdS-sensitized TiO_2. Layers about 5.5 μm thick are applied for sensitization with CdS: SD-SILAR thus revealed to be not just a technique for surface coverage, but it is successful in a volume growth of nanocrystals inside thick mesoporous layers. CdS is homogeneously distributed over the entire film thickness for both bath- and SD-SILAR, indicating that the new technique is able to accurately create the conditions for chemical reaction of precursors over the entire film thickness, and not only at the surface of the sprayed layer.

In order to examine the surface chemical state and composition, XPS measurements (shown in Fig. 5 and Table 2) were performed.

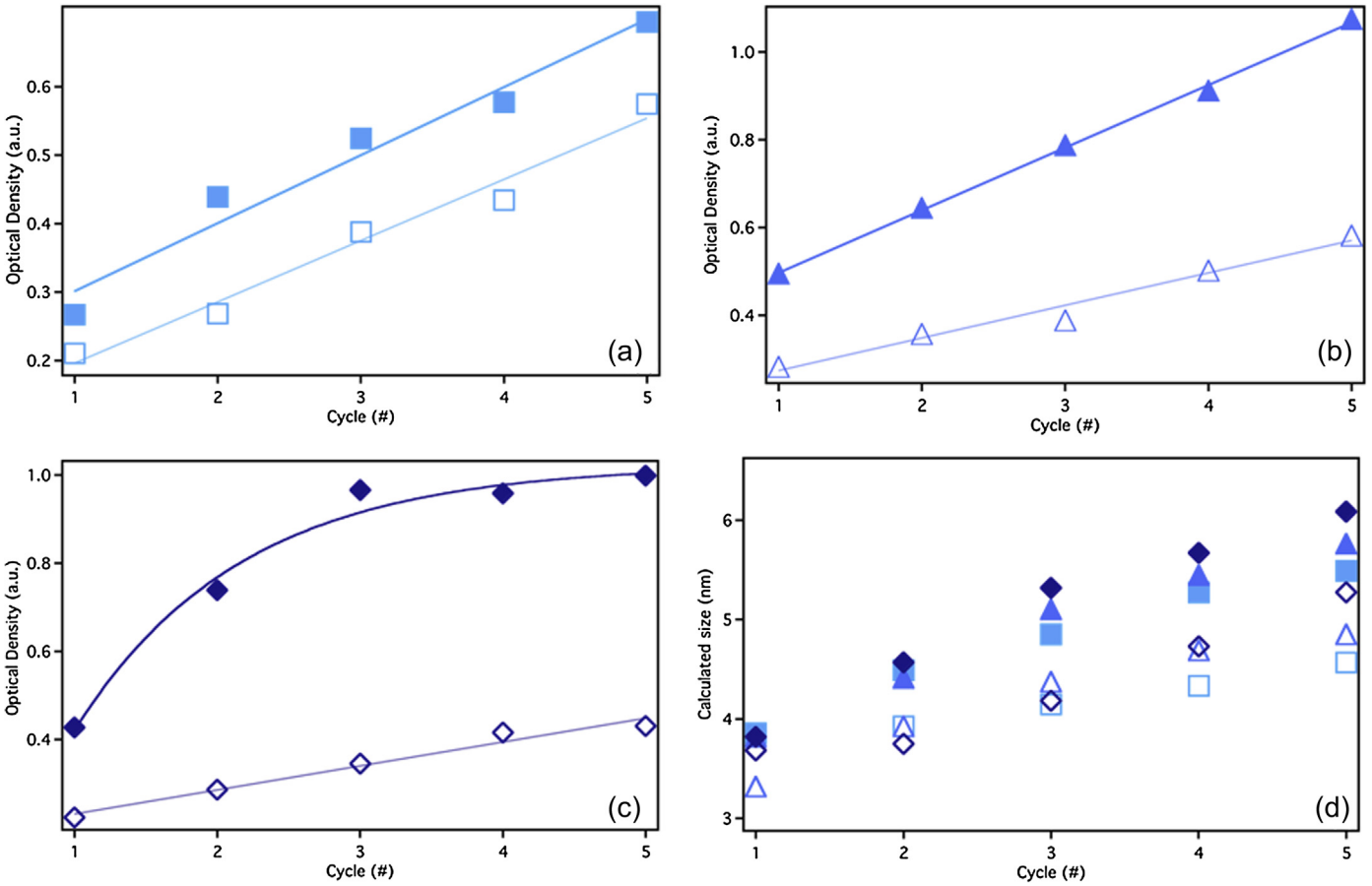

Fig. 3. Effect of applied temperature on NC OD evolution. (a) 40 °C; (b) 50 °C; (c) 60 °C. (d) NC size evolution (fill markers are bath-SILAR and empty markers are SD-SILAR-deposited NCs; squares: 40 °C; triangles: 50 °C; rhombs: 60 °C). Sprayed precursor volume: 0.5 ml. Markers are experimental point; lines are fits. Increasing blue colors are associated to increasing temperatures. (For interpretation of the references to colour in this figure legend, the reader is referred to the web version of this article.)

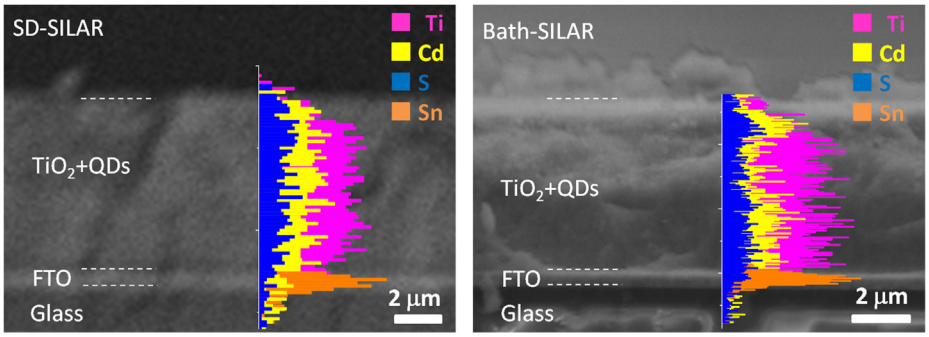

Fig. 4. Cross-section SEM images and related EDS elemental mapping of TiO_2 nanoparticulate film on FTO glass sensitized with CdS QDs via SD-SILAR (left) and bath-SILAR (right). Almost homogeneous in-depth concentration for all the analyzed elements (Ti, Cd, S) has been found in the samples, indicating quite homogeneous nucleation and growth of QDs for both the techniques. The signal pertaining tin from the FTO layer is as well detectable.

Concerning Cd 3*d* core level, binding energies (BEs) values (404.9, 405.1 eV for Cd $3d_{3/2}$ and 411.7, 411.9 eV for Cd $3d_{1/2}$, respectively for SD-SILAR and bath-SILAR) and peak shape are consistent with values reported in literature for Cd(II) [24]. The analysis of S 2*p* XP region revels the presence of sulfur in different environment: the contribution at lower BEs (161.3 and 161.4 eV, respectively for SD- and bath-SILAR) is characteristics of S–Cd bonds in CdS, while the small one at higher BEs (around 168.2 eV), particularly evident in the bath-SILAR sample, is ascribable to sulfate species [25], whose presence is not surprising on naked quantum dots. The presence of sulfate species is also confirmed by O 1*s* spectral region. The analysis of O 1*s* core level reveals the presence of two main contributions. The peak at 529.9 eV is characteristic of O–Ti bond, although contribution of O–Cd species cannot be excluded. Both these species, in fact, fall in a narrow BE range. The shoulder at higher BEs (around 531.6 eV) can be ascribable to both hydroxyl groups and oxygen in sulfate species [25]. Besides the main contribution relative to O–Ti bond (529.9 eV), in fact, a small shoulder around 531.6 eV characteristic of oxygen in sulfate is evident [25]. Peak shape and BEs values measured for Ti 2*p* are consistent with Ti(IV) in TiO_2.

Quantitative XPS analysis evidences that CdS quantum dots are surface enriched in Cd: Cd/S surface atomic ratio is higher than 1 (2.39 and 2.34, respectively for bath- and SD-SILAR). This result is in agreement with a general trend reported in literature in obtaining Cd-enriched QDs [26–28]. This finding could be ascribed to a certain preference of the nanocrystals in having Cd^{2+} ions on surface, which can thus bind the chosen stabilizers agent (i.e. in our case TiO_2). The excess of oxygen respect to titanium (O/Ti atomic ratio considerably higher than the nominal one for TiO_2) seems to support the hypothesis of a Cd–O bond.

Moreover, another important information derived by XP analysis concerns the amount of CdS deposited on TiO_2 surface. Cd/Ti and S/Ti surface atomic ratios reveals that SD-SILAR is most effective in depositing an increased amount of quantum dots on TiO_2 surface, both Cd/Ti and S/Ti surface atomic ratios are, in fact, almost doubled than in bath-SILAR (Table 2), thus confirming the optical measurements.

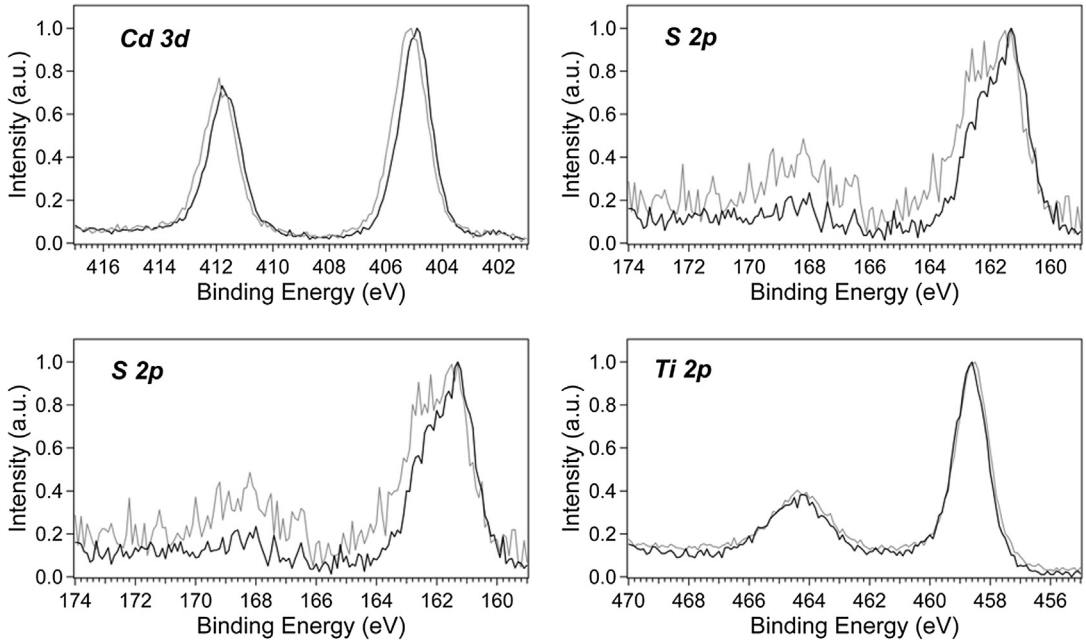

Fig. 5. Cd 3*d*, S 2*p*, O 1*s*, Ti 2*p* XP spectra obtained on the SD-SILAR (black line) and bath-SILAR (grey line) (CdS 5 cycles) (Spectra are normalized with respect to their maximum values).

Table 2
Quantitative XPS analysis of bath-SILAR and SD-SILAR (CdS 5 cycles).

Sample	Cd/Ti	S/Ti	Cd/S	O/Ti
Bath-SILAR	0.55	0.23	2.39	2.9
SD-SILAR	1.03	0.44	2.34	2.8

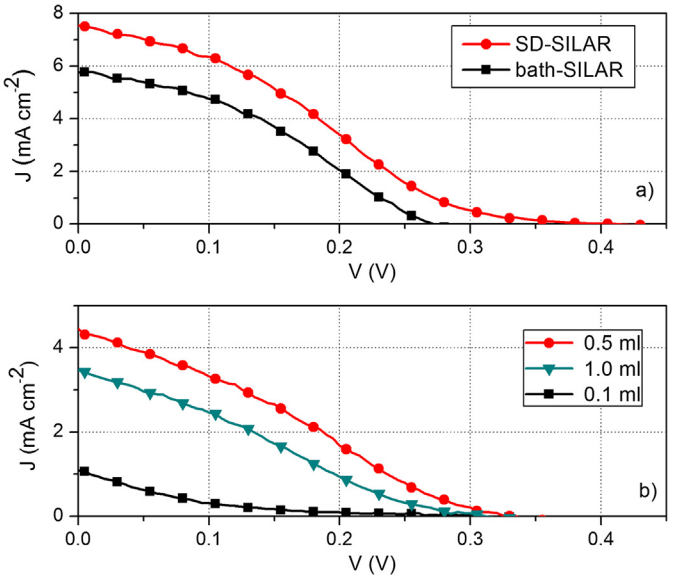

Fig. 6. (a) Current density versus applied voltage curve of CdS-sensitized TiO_2 photoanodes via SD-SILAR and SILAR under one sun irradiation (AM 1.5 G, 100 mW cm^{-2}). (b) Effect of sprayed volume on current density versus voltage curve for CdS-sensitized TiO_2 photoanodes via SD-SILAR.

The comparative analysis of the functional properties of QDSCs using SD- and bath-SILAR is reported in Fig. 6(a) and Table 3 for cells fabricated applying photoanodes with the same thickness. SD-SILAR results in systematically higher photocurrent and photovoltage with respect to SILAR. Photoconversion efficiency up to 40% higher in SD-SILAR has been recorded (0.78% as compared to 0.56%).

The effect of the sprayed volume has been investigated in a series of thin substrates (Fig. 6(b)). It is visible that optimum volume exists (0.5 ml in the specific set-up) to maximize PV performances in terms of both photoinduced current and voltage and photoconversion efficiency, accordingly.

Characteristic electron lifetime (t_e), obtained by transient photovoltage decay [29], is reported for two selected samples in Fig. 7, to elucidate possible difference between spray and bath deposition of QDs on the functional properties of the solar cells. Eq. (2) gives a fast method to calculate directly t_e from the transient photovoltage decay. t_e is intimately related to the nature of the interface oxide/QD/electrolyte.

$$\tau_e = \frac{k_B T}{e}\left(\frac{dV_{oc}}{dt}\right)^{-1} \quad (2)$$

Table 3
Comparison of functional properties obtained from SD- and bath-SILAR sensitized cells.

Sample	d (μm)	V_{OC}	J_{SC} (mA cm^{-2})	FF	PCE (%)
Bath-SILAR	11.5	0.27	5.76	0.36	0.56
SD-SILAR	11.5	0.41	7.55	0.25	0.78

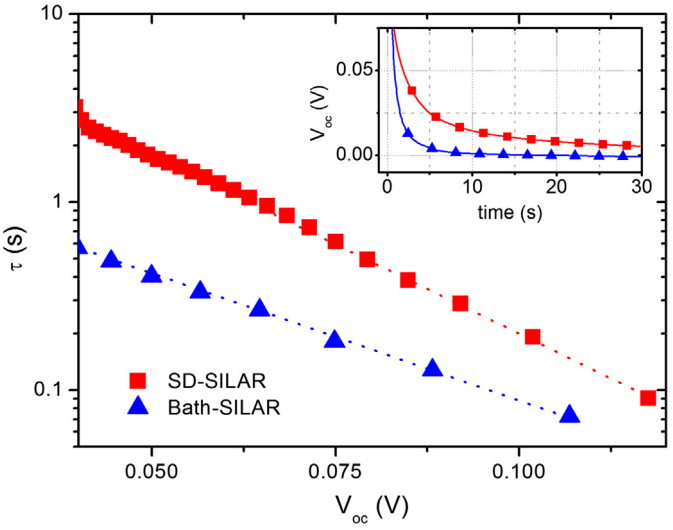

Fig. 7. Electron lifetime versus the open circuit voltage for SD-SILAR and bath-SILAR. Inset: transient photovoltage decay.

where k_B is the Boltzmann constant, T is the absolute temperature, and e is the elementary charge. SD-SILAR results in systematically higher electron lifetime with respect to bath-SILAR. In excitonic solar cells electron lifetime relies on ability of the various

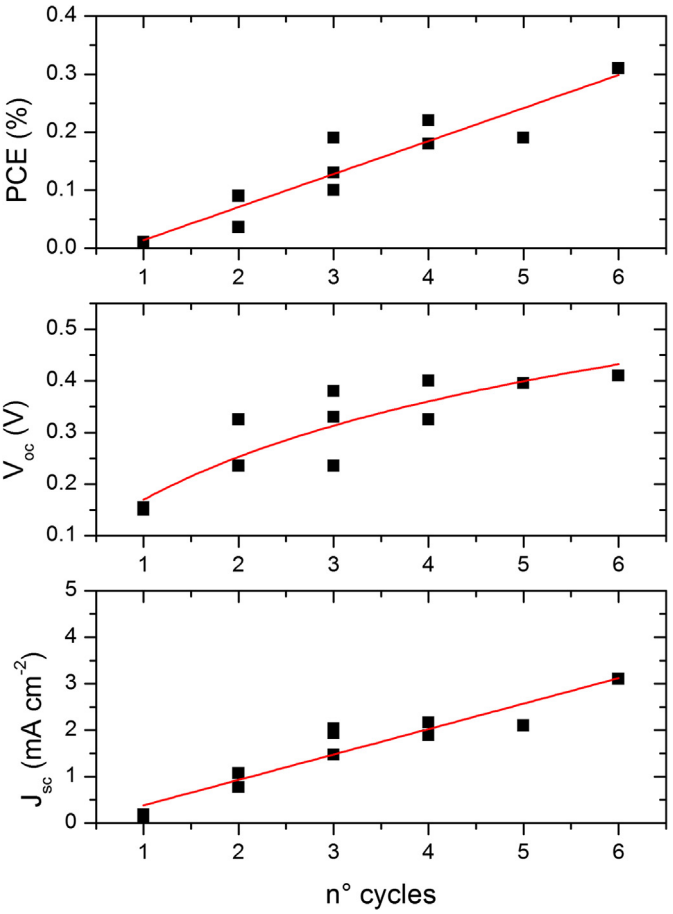

Fig. 8. Top to bottom: PCE, V_{OC} and J_{SC} as a function of SD-SILAR cycles on a batch of 10 solar cells sensitized via CdS QDs. Each cell is capped with a ZnS cycle to improve cell stability.

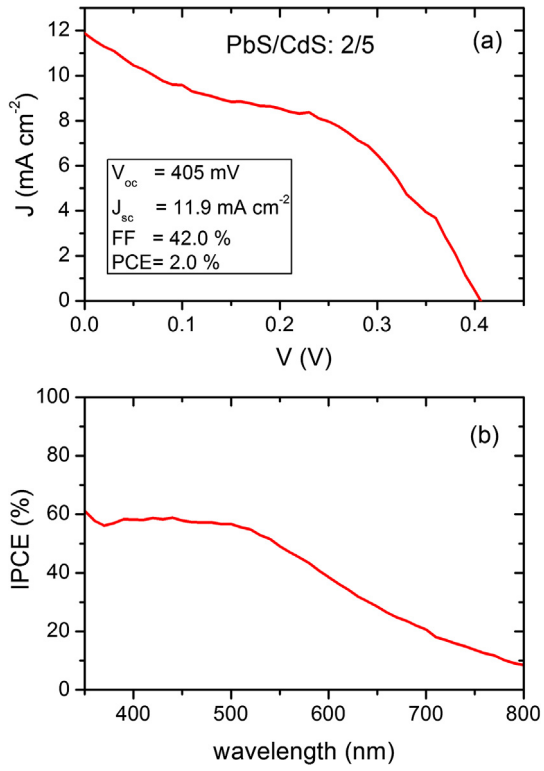

Fig. 9. (a) Current density versus applied voltage curve of TiO_2 photoanode spray-sensitized by two cycles of PbS and 5 cycles of CdS. (b) IPCE of the cell in (a).

components of the cell to fast inject photogenerated electron from the light harvester to the electron transporter, thus reducing recombination probability before charge collection. For this reason, enhanced electron lifetime correlates with improved photoconversion efficiency. In the present case, electron lifetime measurements directly correlate with the functional properties of the solar cell, in which SD-SILAR results in higher photoconversion efficiency with respect to bath-SILAR.

The photovoltaic properties of a series of 10 cells sensitized by CdS SD-SILAR are reported in Fig. 8. A 5 μm thick photoanode has been used. Of course, the choice of thin anode is detrimental for gaining high photoconversion efficiency (15 μm being the optimum thickness for a TiO_2 photoanode), but it allows high reproducibility of the oxide layer, which is critical for proper comparison of QDSCs. Each QD system has been capped with a ZnS SD-SILAR cycle at the end of CdS deposition to prevent QDs from fast degradation [30]. J_{SC} and V_{OC} increase with the number of cycles, as expected from enhanced optical density of the layer, which results in enhanced photo-generated electrons. PCE increases accordingly, of course. High reproducibility of the functional features of the cells can be appreciated, which is a sign of the precise tuning of QD size and size distribution as testified by the optical properties of the sensitized layers. In addition, following consolidated results of our previous work [14], we tried to increase the photoconversion efficiency of the solar cell based on spray deposition by applying a composite PbS/CdS QD system, in which the presence of PbS extends light absorption towards the infrared region. In Fig. 9 the functional properties of the cell are reported. A standard copper sulfide counter electrode is applied. Short circuit photocurrent as high as 11.9 mA cm^{-2} and PCE as high as 2.0% were obtained as a consequence of the broadened light absorption towards the infrared region, as testified by the incident photon to electron photoconversion efficiency (IPCE). Such PCE is one of the highest ever reported for a QDSC based on sulfide QDs and liquid electrolyte, and is extremely promising for the development of QDSCs using spray deposition.

4. Conclusions

This work demonstrates the potential hold by spray deposition applied to SILAR technique in generating and growing semiconductor quantum dots on nanoparticulate metal oxides. With respect to traditional bath-SILAR, spray deposition was found to provide for higher amount of smaller nanocrystals, resulting in increased functional performances of the corresponding solar cells.

The last, although not less relevant, characteristic of the proposed approach worth to be mentioned is the reduced amount of precursors needed to perform SD-SILAR. As previously highlighted, this is highly desirable for both a possible scale up perspective and reduced environmental impact.

Despite this actual potential, before a scale up could be undertaken, it has to be pointed out that issues related to device reliability must be faced. Duration of QDSCs is rarely studied in literature, since the use of both naked nanocrystals and liquid electrolytes pose problems related on one hand to material stability under working conditions and, on the other hand, to leakage of the hole conductor over the time. While stability of nanocrystals can be reasonably improved by applying capping layers, such as ZnS, the seek for alternative, solid electrolytes is more challenging: research community is strongly committed to this goal and recent findings seem rather promising, at least for dye sensitized solar cell [31].

Acknowledgments

IC acknowledges Regione Lombardia under “X-Nano” Project (“Emettitori di elettroni a base di nano tubi di carbonio e nanostrutture di ossidi metallici quasi monodimensionale per lo sviluppo di sorgenti a raggi X”) for funding. GSS thanks OIKOS srl for financial support. AV acknowledges the European Commission under the contracts WIROX (no. 295216) and F-LIGHT (no. 299490) for partial funding.

M.N. Poli and M.S. Crottini are acknowledged for technical support.

References

[1] I.L. Medintz, H.T. Uyeda, E.R. Goldman, H. Mattoussi, Nat. Mater. 4 (2005) 435.
[2] R.C. Somers, M.G. Bawendi, D.G. Nocera, Chem. Soc. Rev. 36 (2007) 579. and references therein.
[3] S. Rühle, M. Shalom, A. Zaban, Chem. Phys. Chem. 11 (2010) 2290.
[4] C.B. Murray, D.J. Norris, M.G. Bawendi, J. Am. Chem. Soc. 115 (1993) 8706.
[5] J.H. Bang, P.V. Kamat, ACS Nano 3 (2009) 1467. and references therein.
[6] A. Shabaev, Al.L. Efros, A.J. Nozik, Nano Lett. 6 (2006) 2856.
[7] A. Yella, H.-W. Lee, H.N. Tsao, C. Yi, A.K. Chandiran, Md.K. Nazeeruddin, E.W.-G. Diau, C.-Y. Yeh, S.M. Zakeeruddin, M. Grätzel, Science 334 (2011) 629.
[8] I. Mora-Sero, S. Gimenez, F. Fabregat-Santiago, R. Gomez, Q. Shen, T. Toyoda, J. Bisquert, Acc. Chem. Res. 42 (2009) 1848.
[9] E.M. Barea, M. Shalom, S. Gimenez, I. Hod, I. Mora-Sero, A. Zaban, J. Bisuert, J. Am. Chem. Soc. 132 (2010) 6834.
[10] P.K. Santra, P.K. Kamat, J. Am. Chem. Soc. 134 (2012) 2508.
[11] M.P. Genovese, I.V. Lightcap, P.V. Kamat, ACS Nano 6 (2012) 865.
[12] Y.-L. Lee, Y.-S. Lo, Adv. Func. Mater. 19 (2009) 604.
[13] H. Lee, M. Wang, P. Chen, D.R. Gamelin, S.M. Zakeeruddin, M. Grätzel, Md.K. Nazeeruddin, Nano Lett. 9 (2009) 4221.
[14] A. Braga, S. Gimenez, I. Concina, A. Vomiero, I. Mora-Seró, J. Phys. Chem. Lett. 2 (2011) 454.
[15] N. Guijarro, T. Lana-Villareal, Q. Shen, T. Toyoda, R. Gomez, J. Phys. Chem. C 114 (2010) 21928.
[16] Y.H. Lee, S.H. Im, J.H. Rhee, J.-H. Lee, S. Il Seok, ACS Appl. Mat. Interfaces 2 (6) (2010) 1648.
[17] S.H. Im, Y.H. Lee, S.W. Kim, S.-W. Kim, Langmuir 26 (23) (2010) 18576.
[18] W.W. Yu, L. Qu, W. Guo, X. Peng, Chem. Mater. 15 (2003) 2854.
[19] (a) D.A. Shirley, Phys. Rev. B 5 (1972) 4709;
(b) J.F. Moulder, W.F. Stickle, P.E. Sobol, K.D. Bomben, in: J. Chastain (Ed.),

Handbook of X-ray Photoelectron Spectroscopy, Physical Electronics, Eden Prairie, MN, 1992.
[20] Z.G. Zhao, Z.-F. Liu, M. Miyauchi, Adv. Func. Mater. 20 (2010) 4162.
[21] O.M. Piepenbrock, T. Stirner, M. O'Neill, S.M. Kelly, J. Am. Chem. Soc. 129 (2007) 767.
[22] I. Concina, M.M. Natile, E. Tondello, G. Sberveglieri, Dalton Trans. 41 (2012) 14354.
[23] F. Sauvage, J.-D. Decoppet, M. Zhang, S.M. Zakeeruddin, P. Comte, M. Nazeeruddin, P. Wang, M. Grätzel, J. Am. Chem. Soc. 133 (2011) 9304.
[24] P.K. Khanna, K. Srinivasa Rao, K.R. Patil, V.N. Singh, B.R. Mehta, J. Nanopart. Res. 12 (2010) 101.
[25] NIST Standard Reference Database 20, Version 3.5 G. Konstantatos, L. Levina, A. Fischer, E.H. Sargent, Nano Lett. 8 (2008) 1446.
[26] J. Taylor, T. Kippeny, S.J. Rosenthal, J. Cluster Sci. 12 (2001) 571.
[27] I. Moreels, B. Fritzinger, J.C. Martins, Z. Hens, J. Am. Chem. Soc. 130 (2008) 15081.
[28] I. Concina, M.M. Natile, M. Ferroni, A. Migliori, V. Morandi, L. Ortolani, A. Vomiero, G. Sberveglieri, Chem. Phys. Chem. 12 (2011) 863.
[29] (a) J. Bisquert, F. Fabregat-Santiago, I. Mora-Sero, G. Garcia-Belmonte, S. Giménez, J. Phys. Chem. C 113 (2009) 17278;
(b) A. Zaban, M. Greenshtein, J. Bisquert, Chem. Phys. Chem. 4 (2003) 859.
[30] N. Guijarro, J.M. Campina, Q. Shen, T. Toyoda, T. Lana-Villareal, R. Gomez, Phys. Chem. Chem. Phys. 13 (2011) 12024.
[31] I. Chung, B. Lee, J. He, R.P.H. Chang, M.G. Kanatzidis, Nature 485 (2012) 486.